higher resolution and further discriminate among possible chemical modifications.

For example, the highly chemoselective activation of carboxyl groups by treatment with *N*-ethyl-*N*′-(3-dimethyl aminopropyl) carbodiimide (EDC) and *N*-hydroxysuccinimide (NHS) is used to attach proteins to carboxy-terminated surfaces via amide linkages (*36*). In a third series of chemical experiments, redox-cycled SWNTs were treated with EDC and NHS in an attempt to covalently link Au-labeled streptavidin to SWNT carboxyls (*37*). Only one attachment was observed on 10 redox-cycled SWNT devices, which shows that the acid treatment does not generally produce sidewall carboxy groups. This result is in agreement with our speculation that ethers are the dominant residual functionality. However, four of nine devices showed protein attachments when additional $KMnO_4$ oxidation was added to the procedure. $KMnO_4$ readily converts hydroxides to carboxy groups, so we can conclude with some certainty that the electronic maps in Fig. 3, B and C, are related to carboxy-functionalized sites.

Figure 4A and fig. S5A show scanning electron micrographs of successful protein attachments. In each image, a single streptavidin-coated Au particle is integrated into a functioning SWNT device. Electrical characterization of these devices shows that each circuit is insulating immediately before streptavidin attachment but conducting afterward (Fig. 4, B to E). G is critically dependent on the presence of the protein, just as in the case of the Ni decorations, even though the current does not flow through the entire protein or gold particle per se. As in Fig. 3E, the measured G reflects the series combination of SWNT band structure and protein-linked oxidation gaps, and these devices could exhibit strong biosensitivity, as previously shown for noncovalently coated SWNTs (*38*).

The usefulness of G to monitor and control chemistry in situ and in real time arises from its sensitivity to a few single-bond redox events. Paradoxically, SWNT devices never drop directly to $G = 0$ without intermediate steps and terraces, and questions remain regarding the exact nature of these terraces. Additional experiments may distinguish among intermediate chemical states, oxidation cascades among neighboring carbon atoms, or other possible mechanisms.

References and Notes

1. G. Maruccio *et al.*, *Electroanalysis* **16**, 1853 (2004).
2. A. A. Tseng, A. Notargiacomo, T. P. Chen, *J. Vac. Sci. Technol. B* **23**, 877 (2005).
3. H. Park, A. K. L. Lim, A. P. Alivisatos, J. Park, P. L. McEuen, *Appl. Phys. Lett.* **75**, 301 (1999).
4. D. R. Strachan *et al.*, *Appl. Phys. Lett.* **86**, 43109 (2005).
5. W. Ho, *J. Chem. Phys.* **117**, 11033 (2002).
6. N. J. Tao, *J. Mater. Chem.* **15**, 3260 (2005).
7. S. Banerjee, T. Hemraj-Benny, S. S. Wong, *Adv. Mater.* **17**, 17 (2005).
8. P. W. Chiu, G. S. Duesberg, U. Dettlaff-Weglikowska, S. Roth, *Appl. Phys. Lett.* **80**, 3811 (2002).
9. Y. X. Zhou, A. T. Johnson, J. Hone, W. F. Smith, *Nano Lett.* **3**, 1371 (2003).
10. M. R. Diehl *et al.*, *ChemPhysChem* **4**, 1335 (2003).
11. X. Guo *et al.*, *Science* **311**, 356 (2006).
12. K. Kinoshita, *Carbon—Electrochemical and Physicochemical Properties* (Wiley Interscience, New York, 1988).
13. G. U. Sumanasekera *et al.*, *J. Phys. Chem. B* **103**, 4292 (1999).
14. R. Graupner *et al.*, *Phys. Chem. Chem. Phys.* **5**, 5472 (2003).
15. M. Burghard, *Surf. Sci. Rep.* **58**, 1 (2005).
16. X. Lu, Z. F. Chen, *Chem. Rev.* **105**, 3643 (2005).
17. J. Zhao *et al.*, *ChemPhysChem* **6**, 598 (2005).
18. Y. W. Son, J. Ihm, M. L. Cohen, S. G. Louie, H. J. Choi, *Phys. Rev. Lett.* **95**, 216602 (2005).
19. Y. S. Lee, M. B. Nardelli, N. Marzari, *Phys. Rev. Lett.* **95**, 076804 (2005).
20. J. Eom *et al.*, *Physica B* **376–377**, 7 (2006).
21. Y.-S. Lee, N. Marzari, *Phys. Rev. Lett.* **97**, 116801 (2006).
22. See supporting material on *Science* Online.
23. J. Mannik, B. R. Goldsmith, A. Kane, P. G. Collins, *Phys. Rev. Lett.* **97**, 016601 (2006).
24. Y. Fan, B. R. Goldsmith, P. G. Collins, *Nat. Mater.* **4**, 906 (2005).
25. M. Krüger, M. R. Buitelaar, T. Nussbaumer, C. Schonenberger, L. Forro, *Appl. Phys. Lett.* **78**, 1291 (2001).
26. S. Rosenblatt *et al.*, *Nano Lett.* **2**, 869 (2002).
27. I. Heller *et al.*, *Nano Lett.* **5**, 137 (2005).
28. J. O. Besenhard, H. Mohwald, J. J. Nickl, *Synth. Met.* **3**, 187 (1981).
29. A. Metrot, J. E. Fischer, *Synth. Met.* **3**, 201 (1981).
30. M. Bockrath *et al.*, *Science* **291**, 283 (2001).
31. S. J. Tans, C. Dekker, *Nature* **404**, 834 (2000).
32. M. Freitag, A. T. Johnson, S. V. Kalinin, D. A. Bonnell, *Phys. Rev. Lett.* **89**, 216801 (2002).
33. A. Bachtold *et al.*, *Phys. Rev. Lett.* **84**, 6082 (2000).
34. H. Park, J. J. Zhao, J. P. Lu, *Nanotechnology* **16**, 635 (2005).
35. H. Pan, Y. P. Feng, J. Y. Lin, *Phys. Rev. B* **70**, 245425 (2004).
36. J. V. Staros, R. W. Wright, D. M. Swingle, *Anal. Biochem.* **156**, 220 (1986).
37. S. S. Wong, E. Joselevich, A. T. Woolley, C. L. Cheung, C. M. Lieber, *Nature* **394**, 52 (1998).
38. A. Star, J. C. P. Gabriel, K. Bradley, G. Gruner, *Nano Lett.* **3**, 459 (2003).

39. We thank J. Mannik and F. Alim for experimental assistance, and our team collaborators R. Penner and N. Allbritton for helpful conversations. Supported by NSF NIRT grant EF-0404057, NSF CAREER grant DMR-023-9842 (P.G.C.), American Chemical Society Petroleum Research Fund grant 39672-G5M (P.G.C.), National Institute of General Medical Sciences grant R01 GM078528-01 (G.A.W.), and National Institute of Allergy and Infectious Diseases grant R43 AI58365-01 (G.A.W.).

Supporting Online Material

www.sciencemag.org/cgi/content/full/315/5808/77/DC1
Materials and Methods
SOM Text
Figs. S1 to S5

19 September 2006; accepted 7 November 2006
10.1126/science.1135303

Counting Low–Copy Number Proteins in a Single Cell

Bo Huang,[1]* Hongkai Wu,[1]† Devaki Bhaya,[2] Arthur Grossman,[2] Sebastien Granier,[3] Brian K. Kobilka,[3] Richard N. Zare[1]‡

We have designed a microfluidic device in which we can manipulate, lyse, label, separate, and quantify the protein contents of a single cell using single-molecule fluorescence counting. Generic labeling of proteins is achieved through fluorescent-antibody binding. The use of cylindrical optics enables high-efficiency (≈60%) counting of molecules in micrometer-sized channels. We used this microfluidic device to quantify β_2 adrenergic receptors expressed in insect cells (SF9). We also analyzed phycobiliprotein contents in individual cyanobacterial cells (*Synechococcus* sp. PCC 7942) and observed marked differences in the levels of specific complexes in cell populations that were grown under nitrogen-depleted conditions.

Single-cell analysis has become a highly attractive tool for investigating cellular contents (*1*). Unlike conventional methods that are performed with large cell populations, this technology avoids the loss of information associated with ensemble averaging. Recent studies have described methods that can quantify specific proteins inside a single cell (*2*–*4*) by means of integrated fluorescence (including confocal microscopy, flow cytometry, and monitoring fluorescent enzymatic products) and, in another instance (*5*), by single-molecule imaging. These techniques restrict analysis to one or perhaps a few species at a time because of the need to resolve fluorescence from different probes. Moreover, their applications are limited in the cases where the cell environment changes the fluorescence of the reporter molecule (e.g., through quenching or resonance energy transfer) or where endogenous fluorescence interferes with the measurements.

We present a different approach based on manipulating, capturing, and lysing a single cell, followed by chemical separation and analysis of the lysate. This approach sacrifices the possibility of monitoring live cells but gains the ability to quantify multiple targets that cannot be distinguished by fluorescence properties alone. Recent achievements—including the analysis of DNA (*6*), amino acid profiles (*7*), and protein fingerprints (*8*)—use either a capillary or a mi-

[1]Department of Chemistry, Stanford University, Stanford, CA 94305-5080, USA. [2]Department of Plant Biology, Carnegie Institution, Stanford, CA 94305, USA. [3]Department of Molecular and Cellular Physiology and Medicine, Stanford University, Stanford, CA 94305-5345, USA.

*Present address: Department of Chemistry and Chemical Biology, Harvard University, Cambridge, MA 02138, USA.
†Present address: Department of Chemistry, Tsinghua University, Beijing 100084, China.
‡To whom correspondence should be addressed. E-mail: zare@stanford.edu

crofluidic platform. Compared with the former platform, microfluidics allows sophisticated cell manipulation and provides the potential for extremely high detection sensitivity as well as high-throughput screening.

Low–copy-number proteins (present at fewer than 1000 molecules per cell) play an important role in cell functioning, including signaling and the regulation of gene expression. Without amplification procedures, their abundance is far below the sensitivity limits of conventional protein analysis methods, such as enzyme-linked immunosorbent assay and mass spectroscopy. To solve this problem, we used single-molecule fluorescence detection, which has been applied to counting DNA or protein molecules in sheathed flows, capillaries, and microfluidic channels (*9*–*11*).

Our single-cell analysis chip for mammalian and insect cells (Fig. 1A) is made of polydimethylsiloxane (PDMS) and has three sections: cell manipulation, electrophoretic separation, and single-molecule counting. For cell manipulation, we used a three-state valve design that has been demonstrated previously (*7*). After the cell was captured in the reaction chamber formed between the three-state valve and a conventional two-state valve, a lysing/labeling buffer was injected into the chamber so that the cell contents were released (Fig. 1B). In our experiment with proteins that are not naturally fluorescent, we used fluorescently labeled antibodies as a generic method to tag target proteins. A nonionic detergent, 1 weight percent (wt%) *n*-dodecyl-β-D-maltoside (DDM), was used as the lysing reagent, which preserved the activity of the antibodies.

After the labeling reaction occurred, the excess labeling reagent was electrophoretically separated from the target proteins. To reduce the transportation loss of the sample, the separation buffer contained 0.1 wt% DDM so that protein adsorption on the hydrophobic PDMS channel walls was essentially suppressed (*12*). A low concentration (~0.005 to ~0.05 wt%) of sodium dodecylsulfate (SDS) was added to generate sufficient electro-osmotic flow by its adsorption to the PDMS surface (*13*). Although we used DDM/SDS separation for all of our experiments, we could have used any other electrophoretic/chromatographic separation method that is compatible with a PDMS microfluidic chip.

At the end of the separation channel, fluorescent molecules were counted by monitoring the number of fluorescence bursts generated when the molecules flowed through a small detection volume. For single-molecule counting, the most common approach to obtaining a high signal-to-noise ratio is to use confocal fluorescence microscopy, but its detection cross section (approximately 500 nm wide by 1 μm high) is much smaller than the cross section of an ordinary microfluidic channel (100 μm by 10 μm), which results in extremely poor detection efficiency (*14*). Several groups have attempted to solve this problem by decreasing the dimensions of the channel or capillary to the nanometer range so that the entire cross section fits into the focus of the confocal microscope (*15*–*17*). Such a small channel dimension, however, could affect the electrophoretic separation of molecules in cell

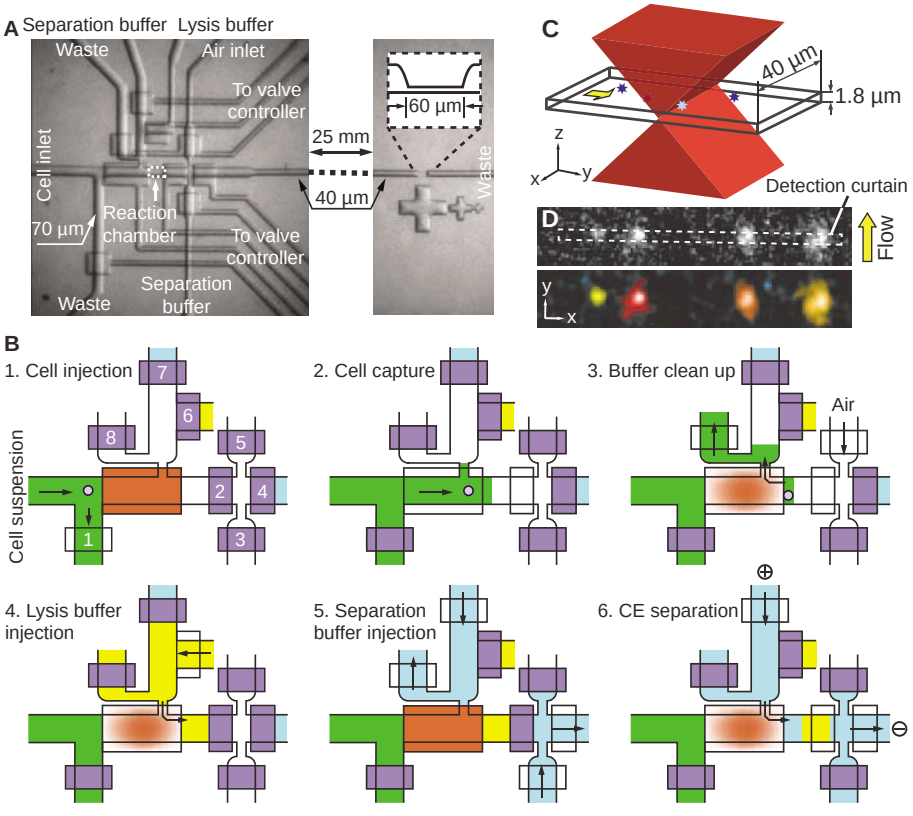

Fig. 1. The single-cell analysis chip. (**A**) Layout of the single-cell chip, showing the cell-manipulation section on the left and the molecule-counting section on the right. (**B**) Analysis procedure for a mammalian or insect cell. (**C**) Schematic illustration of the excitation laser focused by the microscope objective and the dimensions of the molecule-counting channel. (**D**) One frame from the CCD images of fluorescent molecules flowing across the molecule-counting section (upper panel) and the identification results (lower panel).

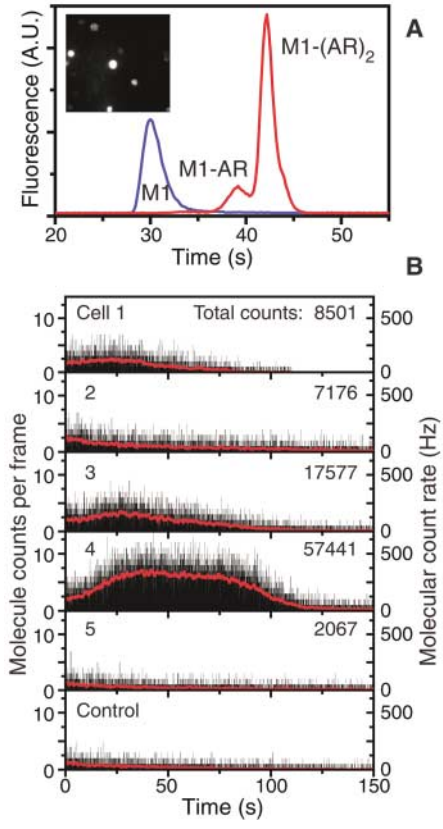

Fig. 2. Analysis of β_2AR in SF9 cells. (**A**) Electropherogram of Cy5-labeled M1 antibody against FLAG (M1); measurements are shown before and after adding an excess amount of purified β_2AR (AR) in a double-T chip. The inset is an image of SF9 cells expressing β_2AR and fluorescently stained with M1. A.U., arbitrary units. (**B**) Molecule-counting results of SF9 cells expressing β_2AR, showing the electropherogram of the M1-AR complexes. The red line represents the average count rate. The total counts are corrected for the counting efficiency, the existence of M1-$(AR)_2$ complexes, and blank counts in the control experiment (5613 molecules). The control experiment was performed by separating lysis/labeling buffer in the reaction chamber with no cells captured. The background counts were mainly caused by the tailing of the large free-antibody peak that came earlier in the electropherogram (not shown).

lysates (*18*, *19*) and could also lead to a clogging of the nanochannel with cell debris.

To resolve the counting-efficiency problem, we widened the excitation laser focus in one direction by using cylindrical optics. The excitation laser beam was focused by a cylindrical lens to form a line at the back focal plane of a high-numerical-aperture objective (fig. S1). When the laser beam emerged from the objective, it was collimated in the direction perpendicular to the channel length so that it illuminated a channel width of tens of micrometers (Fig. 1C). In the other direction, the laser was still tightly focused by the objective to minimize the fluorescence background from out-of-focus excitation. The limit of the channel height by the excitation focus was ~2 μm (fig. S1B), which was slightly relaxed as compared to confocal detection because the laser was less tightly focused. This height was large enough to avoid clogging in our experiments.

With this optical configuration, the excitation laser formed a rectangular, curtain-shaped detection region across the channel. The fluorescence from molecules that passed through the curtain was recorded by an intensified charge-coupled device (CCD) camera. We used a threshold criterion to identify each molecule as a bright spot in an image frame (Fig. 1D). To enhance the fluorescence signal for molecule counting, we slowed down the flow rate when an analyte was expected to pass through the detection curtain.

Because of the variation in excitation laser intensity at different positions in the channel cross section, molecules that passed through the periphery of the channel produced lower fluorescence signals, which could be lost in the background noise. As a result, the detection efficiency varied slightly according to the brightness of a specific sample molecule. We have measured the molecular-counting efficiency of Alexa Fluor 647–labeled streptavidin in a standard double-T chip and found that 60% of the injected molecules are counted (*20*). A general method was then developed to estimate detection efficiencies directly from counting experiments by varying the threshold of molecule identification (*20*). In this way, the actual number of molecules can be derived without additional calibration.

Using the single-cell analysis chip, we quantified the copy number of a human transmembrane protein, β_2 adrenergic receptor (β_2AR), expressed in an insect cell line (SF9). β_2AR is not naturally fluorescent. Therefore, we genetically added a short peptide sequence, the FLAG tag, to the N terminus (*21*), so that it could bind Cy5-labeled monoclonal M1 antibody against FLAG (Cy5-M1) with high affinity (dissociation constant = 2.4 nM) (*22*). The antibody concentration was 20 nM in the lysis/labeling buffer, which caused ~90% of the β_2AR to be fluorescently tagged. β_2AR in SF9 cells can be efficiently extracted with 1 wt% DDM, which is demonstrated by the rapid disappearance of fluorescence from Cy5-M1–stained cells when the lysing buffer is added.

The immunocomplexes of Cy5-M1 and purified β_2AR could be separated with the DDM/SDS system (Fig. 2A). Figure 2B lists the molecule-counting results of five transfected SF9 cells. These cells contained an average of ~1.8×10^4 β_2AR per cell, which was in agreement with the ensemble measurement using cell lysate [4×10^4 β_2AR per cell, detectable by Cy5-M1 binding (*20*)]. The copy numbers of β_2AR in these cells varied between ~2000 and ~60,000. By staining with Cy5-M1 (Fig. 2A, inset), we could observe similar variations in whole-cell fluorescence intensity, although cell staining detects only the β_2AR that is present on the cell surface. This cell-to-cell variation is probably caused by the stochastic nature of virus infection; i.e., individual cells are not infected simultaneously and may contain different numbers of viral particles, resulting in different expression levels of β_2AR.

To demonstrate a biological application of single-cell analysis, we studied the response of the unicellular cyanobacterium *Synechococcus* sp. PCC 7942 (*Synechococcus* hereafter) to the depletion of nitrogen-containing nutrients in the culture medium (chlorosis). Cyanobacteria and some eukaryotic algae use the phycobilisome (PBS), a peripheral membrane protein-chromophore complex, to collect the light energy and transfer it to the photosynthetic reaction centers (*23*). In *Synechococcus* cells, the PBS comprises mainly two pigmented phycobiliproteins (PBPs): phycocyanin (PC), which exists in the peripheral rods, and allophycocyanin (APC), which forms the core structure. It also contains various linker polypeptides that function to hold together the assembly and to tune the complex for efficient energy flow into the photosynthetic reaction centers. A chromophore-containing linker polypeptide designated L_{CM} attaches the PBS to photosystem II on the thylakoid membrane (*23*, *24*).

When grown under conditions in which certain macronutrients (such as nitrogen) are depleted, these cyanobacteria begin to degrade their PBS in an ordered way (first PC, then APC). This process reduces the absorption of excess light energy and provides cells with nutrients from the degraded PBP, helping them to attain a quiescent state almost devoid of the PBS (Fig. 3A, inset) (*23*, *25*). To characterize this process at the ensemble level, we lysed *Synechococcus* that was cultured in nitrogen-replete (+N) or nitrogen-depleted (–N) media using the combination of lysozyme and a nonionic surfactant. The extracted PBP complexes in the lysate were electrophoretically separated on a microfluidic chip. As shown in Fig. 3A, after *Synechococcus* was cultured in a –N medium for more than 72 hours, all peaks related to PC (peaks 1 and 4 to 9) nearly disappeared. The two major PBP peaks that remained correspond to two APC subassemblies in the PBS core (peak 2

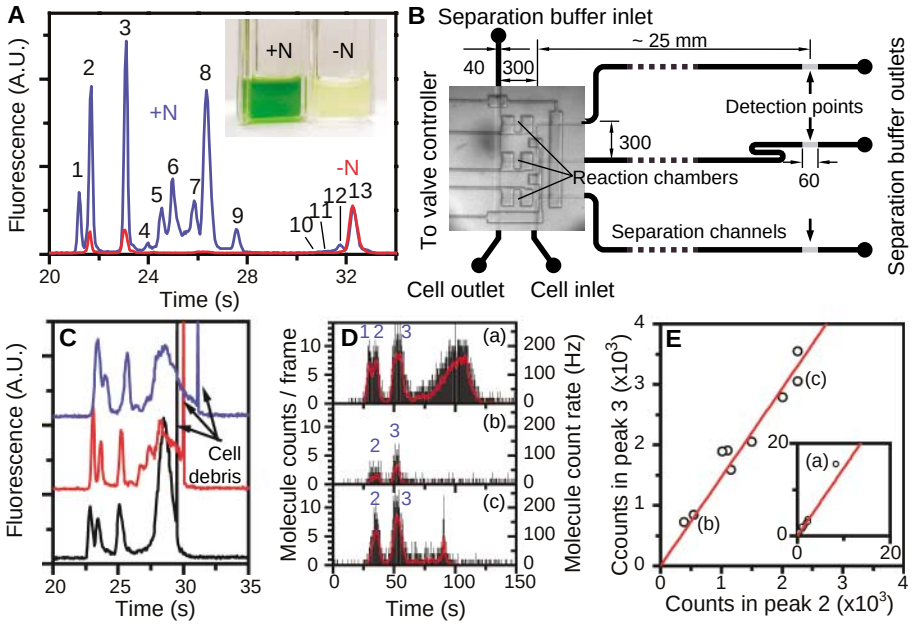

Fig. 3. Single-cell analysis of *Synechococcus* grown in +N and –N culture medium. (**A**) Electropherogram of bulk cell lysates measured in a standard double-T microfluidic chip and normalized to the height of peak 13 (chlorophyll). The inset shows a photograph of the two cell cultures. (**B**) Layout of cyanobacteria analysis chip. Dimensions are in micrometers. (**C**) Electropherograms of phycobiliprotein complexes from three +N cells. The curves are vertically shifted for clarity. (**D**) Molecule-counting results of three –N cells. (**E**) Molecule number distribution of 10 –N cells. The lysing and counting efficiencies are corrected individually. Results from the three cells in (D) are marked by (a), (b), and (c). Red lines show the result of least-square linear fitting. The inset shows cell a, which is excluded from the fitting because its value would dominate the fit.

is the APC-L_{CM} complex and peak 3 is an APC trimer). These observations are consistent with a previously described model for chlorosis (*23*).

Although isolated PC and APC molecules are highly fluorescent, they are difficult to quantify in cells by fluorescence intensities because of the highly efficient energy transfer in the light-harvesting protein complexes, their large spectral overlap, and the fluorescence background from chlorophylls in the photosystems. Our single-cell analysis approach is particularly advantageous because it incorporates chemical separation before fluorescence detection.

We used a chip with three simplified reaction chambers (Fig. 3B) so that up to three cells could be simultaneously lysed. Laser-induced fluorescence detection was used to analyze the +N cells (Fig. 3C) because of their high PBP concentration, whereas molecule counting was used to analyze the –N cells (Fig. 3D). Among the three –N cells shown in Fig. 3D, cell b contains 548 copies of PBP complexes in peak 2 and 839 copies in peak 3, and the detection limit (two times the standard deviation of background counts from noise) is seven molecules. Figure 3E shows the distribution of the molecule numbers of the two PBS core subassemblies (peaks 2 and 3) from 10 –N cells. The cell-to-cell variation in overall PBP counts of –N cells is much larger than that of +N cells. The number of molecules present in these two subassemblies shows a high correlation (r^2 = 0.93) over the entire distribution range. This relation indicates that a constant ratio of these two complexes was maintained during the degradation of the PBS under –N conditions and that, as bleaching of the cells proceeded, the complexes were simultaneously lost. These results suggest coordinated degradation of PBS components within the core of the PBS.

Among the 10 –N cells examined, cell a in Fig. 3D had much brighter fluorescence and much higher molecule counts than the others. Its electropherogram resembled those from +N cells, which indicated an incomplete proteolysis of the PBS. This cell represents those –N cells that have atypically bright fluorescence (~5% of all cells) when observed by fluorescence microscopy. In ensemble experiments in which cell populations are examined, these cells would not be detected because of their low frequencies of appearance. The occurrence of this rare cell could be a consequence of genetic variation within the population, although more work (possibly using *Synechococcus* mutants defective in PBS degradation or using carefully monitored isogenic lines) needs to be done to test this hypothesis.

The method described here should have many applications, making the chemical analysis of single cells by single-molecule counting a new tool for understanding the functioning of cells. Other applications, such as the use of fluorescent proteins that can be genetically fused or the use of dye molecules (such as the biarsenical dye, FlAsH, and its variants) that bind to specific peptide sequences, may further expand the scope of this method to include the monitoring of gene expression and suppression.

References and Notes

1. K. Cottingham, *Anal. Chem.* **76**, 235a (2004).
2. J.-Q. Wu, T. D. Pollard, *Science* **310**, 310 (2005).
3. L. Cai, N. Friedman, X. S. Xie, *Nature* **440**, 358 (2006).
4. J. R. S. Newman *et al.*, *Nature* **441**, 840 (2006).
5. J. Yu, J. Xiao, X. Ren, K. Lao, X. S. Xie, *Science* **311**, 1600 (2006).
6. J. W. Hong, V. Studer, G. Hang, W. F. Anderson, S. R. Quake, *Nat. Biotechnol.* **22**, 435 (2004).
7. H. K. Wu, A. Wheeler, R. N. Zare, *Proc. Natl. Acad. Sci. U.S.A.* **101**, 12809 (2004).
8. S. Hu *et al.*, *Anal. Chem.* **76**, 4044 (2004).
9. A. Castro, F. R. Fairfield, E. B. Shera, *Anal. Chem.* **65**, 849 (1993).
10. D. Chen, N. J. Dovichi, *Anal. Chem.* **68**, 690 (1996).
11. Y. Ma, M. R. Shortreed, H. Li, W. Huang, E. S. Yeung, *Electrophoresis* **22**, 421 (2001).
12. B. Huang, H. Wu, S. Kim, R. N. Zare, *Lab Chip* **5**, 1005 (2005).
13. G. Ocvirk *et al.*, *Electrophoresis* **21**, 107 (2000).
14. B. B. Haab, R. A. Mathies, *Anal. Chem.* **71**, 5137 (1999).
15. W. A. Lyon, S. Nie, *Anal. Chem.* **69**, 3400 (1997).
16. A. Lundqvist, D. T. Chiu, O. Orwar, *Electrophoresis* **24**, 1737 (2003).
17. M. Foquet, J. Korlach, W. R. Zipfel, W. W. Webb, H. G. Craighead, *Anal. Chem.* **76**, 1618 (2004).
18. S. Pennathur, J. G. Santiago, *Anal. Chem.* **77**, 6772 (2005).
19. S. Pennathur, J. G. Santiago, *Anal. Chem.* **77**, 6782 (2005).
20. Materials and methods are available as supporting material on *Science* Online.
21. B. K. Kobilka, *Anal. Biochem.* **231**, 269 (1995).
22. R. J. Whelan *et al.*, *Anal. Chem.* **74**, 4570 (2002).
23. A. R. Grossman, M. R. Schaefer, G. G. Chiang, J. L. Collier, *Microbiol. Rev.* **57**, 725 (1993).
24. A. N. Glazer, D. J. Lundell, G. Yamanaka, R. C. Williams, *Ann. Inst. Pasteur Microbiol.* **B134**, 159 (1983).
25. G. Yamanaka, A. N. Glazer, *Arch. Microbiol.* **124**, 39 (1980).

26. We thank F. S. Thai and X. Yao for the SF9 cell culture, F. Fazeli for the cyanobacteria culture, S. Bailey for purifying the PBS, X. Shi for helping in absorption spectra measurement, and Stanford Nanofabrication Facilities for providing the photolithography equipment. Supported by NSF through grant BES-0508531.

Supporting Online Material

www.sciencemag.org/cgi/content/full/315/5808/81/DC1
Materials and Methods
Figs. S1 to S6
Table S1
References
Movies S1 and S2

17 August 2006; accepted 10 November 2006
10.1126/science.1133992

Mass-Independent Sulfur Isotopic Compositions in Stratospheric Volcanic Eruptions

Mélanie Baroni,[1]* Mark H. Thiemens,[2] Robert J. Delmas,[1] Joël Savarino[1]*

The observed mass-independent sulfur isotopic composition ($\Delta^{33}S$) of volcanic sulfate from the Agung (March 1963) and Pinatubo (June 1991) eruptions recorded in the Antarctic snow provides a mechanism for documenting stratospheric events. The sign of $\Delta^{33}S$ changes over time from an initial positive component to a negative value. $\Delta^{33}S$ is created during photochemical oxidation of sulfur dioxide to sulfuric acid on a monthly time scale, which indicates a fast process. The reproducibility of the results reveals that $\Delta^{33}S$ is a reliable tracer to chemically identify atmospheric processes involved during stratospheric volcanism.

Plinian volcanic eruptions dramatically modify climate for several years by injecting large amounts of dust and gases, such as sulfur dioxide (SO_2), directly into the stratosphere. Therefore, studying the impact of such eruptions can provide insights into atmospheric chemical sensitivity. The sulfuric acid (H_2SO_4) layer that formed from SO_2 oxidation, within about 1 month for moderate eruptions (*1*, *2*), reflects solar radiation and alters the radiative properties of the atmosphere, cooling the global troposphere (*1*). Satellite observations (*3*) or light detection and ranging measurements (*1*) allow recent volcanic events to be monitored, but the existing volcanic observations database is insufficient to represent all past eruptions (*1*), and it remains difficult to include volcanic events as a climatic forcing parameter in efforts to understand past climates and to predict the impact of future eruptions. An important step in understanding the climatic impact of volcanic events of different sizes is to identify the chemical processes linked to stratospheric eruptions. During these events, the chemical composition of the atmosphere is strongly perturbed, especially the sulfur budget. The magnitude and character of the perturbation depend on parameters such as eruption strength, sulfur loading, altitude of the volcanic plume, latitude of the volcano, and time of year.

The sulfate concentration of ice cores has proven to be a useful chemical proxy of past vol-

[1]Laboratoire de Glaciologie et Géophysique de l'Environnement, CNRS/Université Joseph Fourier, 38400 St. Martin d'Hères, France. [2]Department of Chemistry and Biochemistry, University of California, San Diego, La Jolla, CA 92093–0356, USA.

*To whom correspondence should be addressed. E-mail: baroni@lgge.obs.ujf-grenoble.fr (M.B.); jsavarino@lgge.obs.ujf-grenoble.fr (J.S.)